ACS OMEGA

Open Access

http://pubs.acs.org/journal/acsodf

Article

Tuning the Cerium-Based Metal−Organic Framework Formation by Template Effect and Precursor Selection

Dimitry Grebenyuk, Maria Shaulskaya, Artem Shevchenko, Mirijam Zobel, Marina Tedeeva, Alexander Kustov, Ilia Sadykov, and Dmitry Tsymbarenko*

Cite This: *ACS Omega* 2023, 8, 48394−48404

Read Online

ACCESS | Metrics & More | Article Recommendations | Supporting Information

ABSTRACT: The novel metal−organic framework $[(CH_3)_2NH_2]_2[Ce_2(bdc)_4(DMF)_2]\cdot 2H_2O$ (**Ce-MOF**, H_2bdc—terephthalic acid, DMF—*N*,*N*-dimethylformamide) was synthesized by a simple solvothermal method. **Ce-MOF** has 3D connectivity of **bcu** type with a dinuclear fragment connected with eight neighbors, while three types of guest species are residing in its pores: water, DMF, and dimethylammonium cations. Dimethylamine was demonstrated to have a decisive templating effect on the formation of **Ce-MOF**, as its deliberate addition to the solvothermal reaction allows the reproducible synthesis of the new framework. Otherwise, the previously reported MOF $Ce_5(bdc)_{7.5}(DMF)_4$ (**Ce5**) or its composite with nano-CeO_2 (CeO_2@**Ce5**) was obtained. Various Ce carboxylate precursors and synthetic conditions were explored to evidence the major stability of **Ce-MOF** and **Ce5** within the Ce carboxylate-H_2bdc-DMF system. The choice of precursor impacts the surface area of **Ce-MOF** and thus its reactivity in an oxidative atmosphere. The *in situ* PXRD and TG-DTA-MS study of **Ce-MOF** in a nonoxidative atmosphere demonstrates that it eliminates H_2O and DMF along with $(CH_3)_2NH$ guest species in two distinct stages at 70 and 250 °C, respectively, yielding $[Ce_2(bdc)_3(H_2bdc)]$. The H_2bdc molecule is removed at 350 °C with the formation of novel modification of $Ce_2(bdc)_3$, which is stable at least up to 450 °C. According to the total X-ray scattering study with pair distribution function analysis, the most pronounced local structure transformation occurs upon departure of DMF and $(CH_3)_2NH$ guest species, which is in line with the *in situ* PXRD experiment. In an oxidative atmosphere, **Ce-MOF** undergoes combustion to CeO_2 at a temperature as low as 390 °C. MOF-derived CeO_2 from **Ce-MOF**, **Ce5**, and CeO_2@**Ce5** exhibits catalytic activity in the CO oxidation reaction.

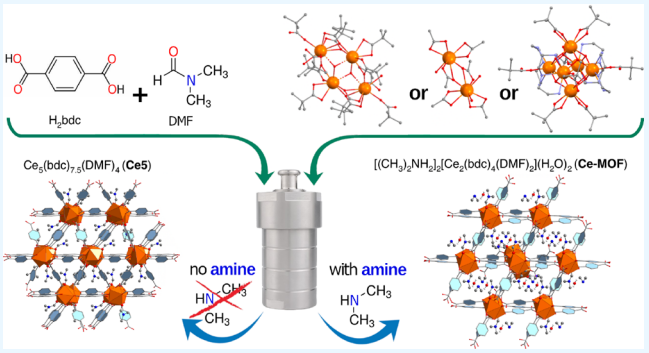

1. INTRODUCTION

Metal−organic frameworks (MOFs) draw substantial attention from many scientific groups nowadays. The main features of MOFs—high surface area and porosity—provide a wide range of potential applications such as gas storage and separation,[1−3] sensing,[4−7] capture of toxic metals,[8,9] drug delivery,[10,11] or catalysis[12−18] including photo-[19,20] and electrocatalysis.[21,22] Terephthalic acid (1,4-benzenedicarboxylic acid, H_2bdc) is a simple rigid ditopic linker often employed for construction of MOFs with several milestone examples such as $Zn_4O(bdc)_3$ (MOF-5),[23] $Cr(OH)(bdc)$ (MIL-53),[24] or $Zr_6O_4(OH)_4(bdc)_6$ (UiO-66).[25]

Lanthanide (Ln) MOFs are attracting increasing attention due to their specific geometrical features that provide wide possibilities of topology design and interesting properties related to magnetic and luminescent applications.[26−28] Despite the progress in the field and tens of thousands of MOFs reported to date,[29] even simple systems such as Ln-H_2bdc have yet to be fully explored. Very recent developments on new Ln-based MOFs with terephthalic linkers still continue to emerge.[30−32]

Cerium MOFs are of particular interest among the Ln-based MOFs due to the unique electronic properties of the Ce ion featuring two stable oxidation states (+3 and +4) and enabling new possible applications as catalysts in various redox processes due to Ce^{3+}/Ce^{4+} switching.,[33−37] e.g., for CO conversion to CO_2.[33,38,39] Like other lanthanides, Ce can adopt various coordination environments. Therefore, the search for new deliberate and reproducible synthetic methods for Ce MOFs is a challenging task. A high number of Ce^{4+} MOFs have been synthesized to date.[40] The majority of them contain *in situ* assembled $\{Ce^{IV}_6O_4(OH)_4\}$ cores and are the most

Received: October 12, 2023
Revised: November 14, 2023
Accepted: November 17, 2023
Published: December 7, 2023

Table 1. Summary of Ce^{3+} MOFs with Terephthalate Linkers Reported in Literature with Porosity Analysis Performed with PLATON[a46]

formula	building unit	free volume (%)	free volume desolvated (%)	CCDC ref code	CCDC number	ref
$Ce_6(bdc)_9(DMF)_9(H_2O)_3$	chain	26.9	49.1	ALUJIB	745286	30
$Ce_5(bdc)_{7.5}(DMF)_4$ (**Ce5**)	chain	29.6	43.0	GOBXAY	912350	31
$Ce_2(bdc)_3(DEF)_2$	chain	30.3	51.3	QOCSAD	630356	47
$[(CH_3)_2NH_2]_2[Ce_2(bdc)_4(DMF)_2]\cdot 2H_2O$ (**Ce-MOF**)	dinuclear	32.3	52.7		2106041	this work
$Ce_2(bdc)_3(DMF)_2(DMSO)_2$	dinuclear	31.9	56.2	BUVHEH	844407	48
$Ce_2(bdc)_3(e\text{-}urea)_2(H_2O)_2$	dinuclear	28.0	45.6	LAGPOA	786945	49
$Ce_2(bdc)_2(NMP)_4(ac)_2$	dinuclear	28.2	60.4	UNECEX	868529	50

[a]Abbreviations for ligands: H_2bdc—terephthalic acid; DMF—*N*,*N*-dimethylformamide, DMSO—dimethyl sulfoxide, e-urea—ethylene urea, DEF—*N*,*N*-diethylformamide, NMP—*N*-methyl pyrrolidone, Hac—acetic acid.

extensively studied after the preparation of the Ce-UiO-66 isoreticular analog of the corresponding Zr-based UiO-66 MOF.[41] MOFs based on Ce^{3+} usually contain mono-,[42,43] di-,[44,48,49] or 1D chain polynuclear[30,31,45,47] building blocks connected by organic linkers. A handful of Ce^{3+} MOFs with nonsubstituted terephthalate linkers have been reported to date (Table 1).

Anionic MOFs are of particular interest through the possibility of sensing and separation of charged species, protonic conduction,[51−53] dye absorption,[54] and capture of toxic metals.[55] A vast number of the reported anionic MOFs contain dimethylammonium cations generated *in situ* via degradation of dimethylformamide usually employed as the solvent for MOF synthesis, e.g., $\{[((CH_3)_2NH_2)_3(SO_4)]_2[Zn_2(ox)_3]\}_n$ (ox = oxalate),[52] $[(CH_3)_2NH_2]_2[Cd_3(L)]\cdot 2H_2O$ (H_4L = 2,5′-di(3′,5′-dicarboxylphenyl)pyridine),[53] and $\{[((CH_3)_2NH_2)_2]$-$[Zn_3(L)_2]\cdot 9H_2O\}$ (L = 5,5′-(1,4-phenylenebis(methylene))-bis(oxy)diisophthalic acid).[55] This potentially decreases synthesis reproducibility with uncontrollable generation of dimethylammonium, as to the best of our knowledge none of the reported synthetic methods employ deliberate addition of dimethylamine to the synthetic mixture.

CO is a toxic gas that is generated by incomplete combustion of fuel from various sources, such as power plants, cement plants, vehicle exhaust emissions, and burning biomass. During CO oxidation, catalysts based on noble metals showed the highest catalytic activity and stability, even at low temperatures.[56] However, there are several disadvantages: low abundance, high price, and stringent requirements for the catalyst preparation process. Therefore, the development of highly active and inexpensive CO oxidation catalysts to replace precious metal catalysts is of great importance for large-scale applications. It is known that the excellent catalytic activity of cerium dioxide catalysts in the CO oxidation reaction can be achieved due to oxygen vacancies on the catalyst surface forming upon synthesis of nanoceria. Recently, MOF-derived ceria-based catalysts in the CO oxidation reaction have become a good substitute for precious metal catalysts due to their low price, large reserves, and high catalytic activity.[33] Therefore, the exploration of new synthetic pathways to produce ceria for catalytic purposes is an urgent matter.

In this article, we have developed a new approach for the synthesis of anionic MOFs containing dimethylammonium cations. We report on the synthesis of the Ce-based MOF $[(CH_3)_2NH_2]_2[Ce_2(bdc)_4(DMF)_2]\cdot 2H_2O$ (**Ce-MOF**) and fine-tuning of synthetic conditions leading to this new target compound in the Ln-H_2bdc-DMF system. The crystal structure of **Ce-MOF** was determined by means of single-crystal X-ray diffraction and by PXRD with Rietveld refinement, supported by pair distribution function (PDF) analysis. TGA-DTA-MS, *in situ* PXRD, and BET add insight on the porosity, specific surface area, and solvent content of the MOF. The effect of the precursor selection on the surface area, reactivity in oxidative conditions, and catalytic activity of MOF-derived CeO_2 in CO oxidation reaction is also reported.

2. EXPERIMENTAL SECTION

Cerium nitrate $Ce(NO_3)_3\cdot 6H_2O$ (99%, Sigma-Aldrich), cerium acetate $Ce(CH_3COO)_3\cdot 1.5H_2O$ (analytical grade, Reakhim, Russia), terephthalic acid (H_2bdc, 98%, Sigma-Aldrich), diethylenetriamine (deta, 99%, Sigma-Aldrich), dimethylamine (33% aq solution, Reakhim, Russia), *N*,*N*-dimethylformamide (DMF, 99.9%, Ekos-1, Russia), pivalic acid (Hpiv, 98%, Merck), and NaOH (analytical grade, Reakhim, Russia) were used as received. Ce(III) hydroxo pivalate $Ce_4(OH)_2(piv)_{10}(H_2O)_2$ and Ce(IV) oxo pivalate $Ce_6O_8(piv)_8(deta)_4$ were synthesized according to previously reported methods.[57,58]

One general method was employed to prepare $[(CH_3)_2NH_2]_2[Ce_2(bdc)_4(DMF)_2]\cdot 2H_2O$ (**Ce-MOF**), differing only in the precursor compound and its amount. A mixture of H_2bdc (136 mg, 0.8 mmol) and (i) $Ce_4(OH)_2(piv)_{10}(H_2O)_2$ (170 mg, 0.1 mmol), (ii) $Ce(CH_3COO)_3\cdot 1.5H_2O$ (136 mg, 0.4 mmol), (iii) $Ce_6O_8(piv)_8(deta)_4$ (150 mg, 0.07 mmol), or (iv) $Ce(NO_3)_3\cdot 6H_2O$ (178.5 mg, 0.4 mmol) was dispersed in DMF (12 mL). Then, dimethylamine water solution (340 μL, 2 mmol) was added and the mixture was placed in Teflon-lined stainless-steel reactors (23 mL), heated at 120 °C for 48 h, and then cooled to room temperature for 24 h. The resulting powder was filtered off, washed with DMF and ethanol, dried, and stored in air. Yield was determined to be ca. 80%.

$Ce_5(bdc)_{7.5}(DMF)_4$ (**Ce5**) was prepared from H_2bdc and (i) $Ce_4(OH)_2(piv)_{10}(H_2O)_2$ or (ii) $Ce(CH_3COO)_3\cdot 1.5H_2O$ by the same method as described above in the absence of dimethylamine. Yield was ca. 60%.

The CeO_2@**Ce5** composite was prepared from H_2bdc and (iii) $Ce_6O_8(piv)_8(deta)_4$ by the same method as described above in the absence of dimethylamine. The yield was ca. 50%.

Single crystals of **Ce-MOF** for X-ray structure analysis were serendipitously obtained during the optimization of the preparation method of **Ce5**.

https://doi.org/10.1021/acsomega.3c07906
ACS Omega 2023, 8, 48394−48404

Scheme 1. Synthetic Scheme of Ce-MOF and Ce5 Preparation from Various Ce Carboxylate Precursors[a]

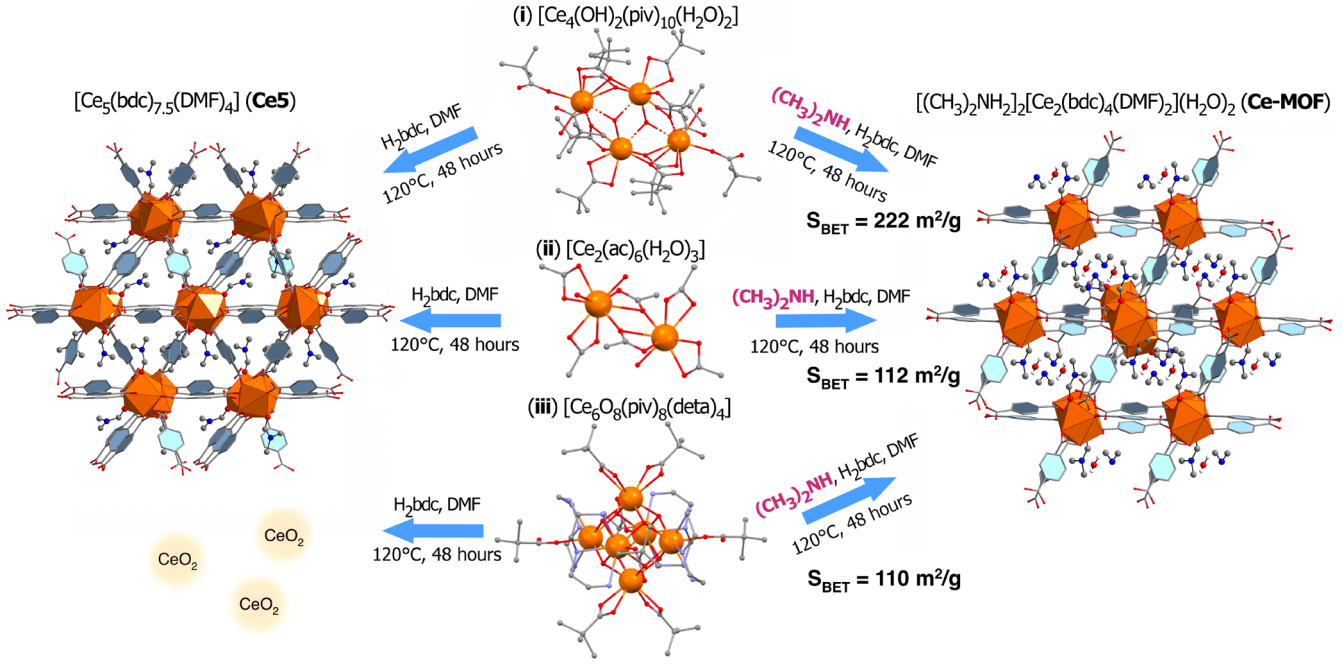

[a] S_{BET} values refer to the desolvated **Ce-MOF** samples obtained from the respective precursors.

3. RESULTS AND DISCUSSION

3.1. General Remarks on Synthesis. Recently, we have elaborated the synthetic routes for tetranuclear $\{Ln_4(OH)_2\}$, $\{Ln_4(OH)_4\}$ and hexanuclear $\{Ce_6O_8\}$, $\{Ln_6(OH)_8\}$ lanthanide carboxylate complexes.[57−59] The intent of the current study was to examine the possibility of creating new MOFs by linking the di-, tetra-, and hexanuclear Ce complexes into an extended 3D framework via the terephthalate linker.

The compounds $[(CH_3)_2NH_2]_2[Ce_2(bdc)_4(DMF)_2]\cdot 2H_2O$ (**Ce-MOF**) and previously reported $Ce_5(bdc)_{7.5}(DMF)_4$[31] (**Ce5**) were successfully synthesized by solvothermal method from terephthalic acid (H_2bdc) and three different Ce carboxylate precursors, (i) $Ce_4(OH)_2(piv)_{10}(H_2O)_2$, or (ii) $Ce(CH_3COO)_3\cdot 1.5H_2O$, or (iii) $Ce_6O_8(piv)_8(deta)_4$, in DMF as outlined in Scheme 1.

The solvothermal reaction that is usually employed for preparation of MOFs is carried out at a relatively high temperature and autogenous pressure of the solvent. Even a slight change in reaction conditions (temperature, pH, presence of modulating reactant) may guide it to a different product.[60,61]

Apart from the desired reaction, interfering processes could occur, including decomposition of the compounds. Accordingly, *in situ* generated dimethylammonium cation $(CH_3)_2NH_2^+$ is a frequent guest in many anionic MOF crystal structures due to the solvent (DMF) decomposition in the temperature range of 100−160 °C.[62−70]

Indeed, in the present work, several serendipitously formed single crystals of the **Ce-MOF** byproduct were harvested from the reaction product of solvothermal synthesis between $Ce_6O_8(piv)_8(deta)_4$ and H_2bdc in DMF, while the main precipitate was the composite CeO_2@**Ce5**. As in previous works, the $(CH_3)_2NH_2^+$ ions have formed due to hydrolysis of DMF in the presence of water traces and acted as a template for the framework assembly (see Section 3.4). However, out-of-control hydrolysis of DMF complicates the synthesis of pure **Ce-MOF** powder in high yield. We have varied the Ce-containing precursor (i−iii), as well as temperature (120−160 °C), time (2−48 h), and reagent concentration in solvothermal syntheses, but most of the syntheses resulted in formation of **Ce5**. The only rigorous and easy way to reproducible synthesis of **Ce-MOF** was discovered to be the deliberate addition of $(CH_3)_2NH$ excess into the reaction vessel. In our view, this novel approach opens the prospect for reproducible synthesis of a large variety of new and previously reported anionic MOFs on templating $(CH_3)_2NH_2^+$ and related cations.

3.2. Synthesis and Characterization of Ce5 and CeO_2@Ce5. We found that the reaction between terephthalic acid (H_2bdc) and either (i) $Ce_4(OH)_2(piv)_{10}(H_2O)_2$,[57] (ii) $Ce_2(ac)_6(H_2O)_3$, or (iii) $Ce_6O_8(piv)_8(deta)_4$[58] in DMF under a broad range of solvothermal conditions leads to formation of a previously reported stable Ce^{3+}-based MOF $Ce_5(bdc)_{7.5}(DMF)_4$ (**Ce5**) (Scheme 1 and Figure S1).[31,71]

Notably, if $Ce_6O_8(piv)_8(deta)_4$ is used as a precursor, Ce^{4+} is only partially reduced to Ce^{3+} and the reaction leads to the formation of a CeO_2@**Ce5** composite, according to PXRD data (Figure 1). The possible mechanism includes reduction of Ce^{4+} to Ce^{3+} by deta, which can be readily oxidized to form polyamines (Figure S2).[72,73] Such types of CeO_2/MOF-based composites are currently studied as catalysts having a prospect to enhance catalytic activity and selectivity.[74,75]

The broad peaks on the experimental PXRD pattern corresponding to CeO_2 reflect the nanoscale state of the particles in the composite. This is supported by the results of scanning electron microscopy (Figure S3), indicating that nano-CeO_2 is distributed on the surface of **Ce5** crystals. Total X-ray scattering with PDF analysis demonstrated that the experimental PDF is in good agreement with the theoretical one of CeO_2 nanoparticles (Figure 2).

The average particle size of the nanomaterial can be deduced from the PDF being a histogram of interatomic distances as the distance at which the curve flattens out since the particle

https://doi.org/10.1021/acsomega.3c07906
ACS Omega 2023, 8, 48394−48404

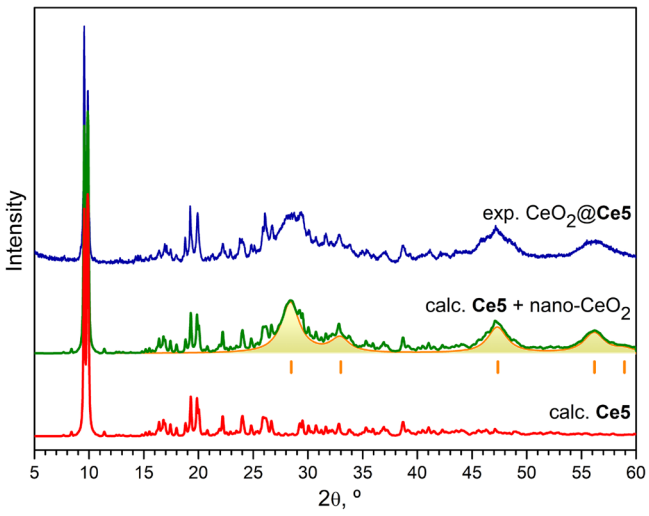

Figure 1. Experimental PXRD pattern (λ = 1.5419 Å) of CeO_2@**Ce5** (blue) and calculated patterns of **Ce5** (red), nano-CeO_2 (yellow), and their composition **Ce5**+nano-CeO_2 (green). Peak broadening of the nano-CeO_2 pattern was calculated for a grain size of 4.5 nm according to the Scherrer equation. Vertical orange bars show the positions of the Bragg peaks of CeO_2.

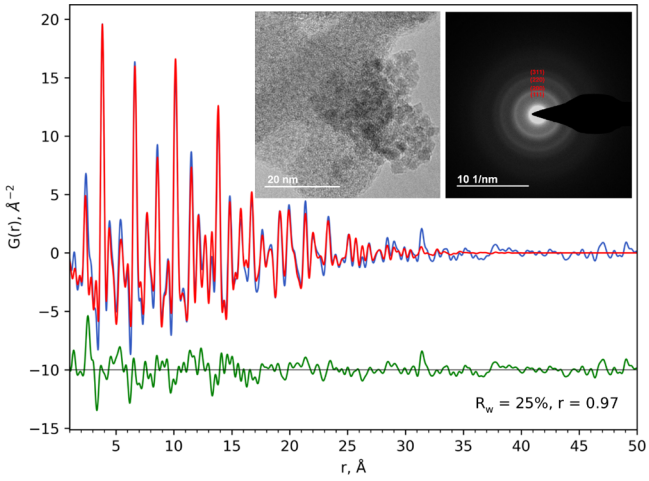

Figure 2. PDF refinement (red) of measured data of CeO_2@**Ce5** (blue) with the CeO_2 spherical particle model for the distance range 1−50 Å. Difference curve (green) is offset for clarity. Weighted agreement factor R_w and Pearson correlation coefficient r between the experimental and fitted curve are shown below the graphs. Insets show the TEM image of the composite (left) and selected-area diffraction pattern with clearly visible diffraction rings corresponding to CeO_2 (right).

diameter is reached, and no interatomic distances exist any further. The CeO_2 particle size value of 4.5 nm was obtained by the PDF fit using a spherical shape function and is in line with the results of transmission electron microscopy (Figure 2).

It should be noted that the CeO_2 signal dominates the PDF despite the comparable amounts of individual phases in CeO_2@**Ce5** (Synthesis section in the SI). The reason for this lies in the higher frequency of Ce−O and Ce−Ce distances in CeO_2 involving the strong scatterer Ce compared to many light scatterers (H, C, O, N) in **Ce5** making the **Ce5** signal hardly visible on the PDF of the composite. Yet, the structural remnants can be seen in the difference curve (Figure S4).

XANES spectra of Ce^{3+} near its L_3 edge (Figure 3) feature a single strong peak at 5726 eV, whereas those of Ce^{4+} have two

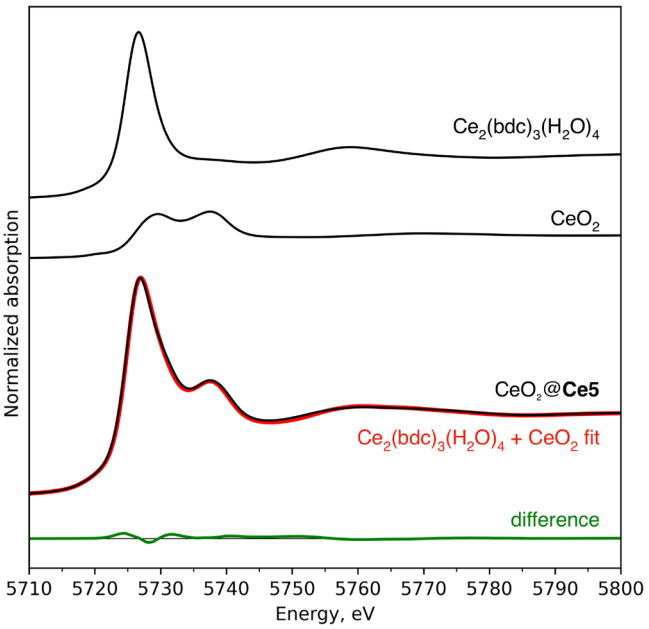

Figure 3. X-ray absorption near edge structure (XANES) spectra of CeO_2@**Ce5** recorded near the Ce L_3 absorption edge fitted with experimental spectra of the model compounds $Ce_2(bdc)_3(H_2O)_4$ and CeO_2.

maxima of lower intensity at 5730 and 5739 eV. The experimental spectrum of CeO_2@**Ce5** can be represented as a sum of the two components, confirming the presence of Ce in both oxidation states. The fitting of XANES spectra of model compounds to the spectrum of CeO_2@**Ce5** estimates the Ce^{3+}:Ce^{4+} molar ratio as 0.47 ± 0.01:0.53 ± 0.01.

3.3. Synthesis of Ce-MOF. Inspired by a serendipitous formation of several **Ce-MOF** crystals as a byproduct due to hydrolysis of DMF, we decided to deliberately add the templating $(CH_3)_2NH$ to the reaction mixture. This led to the formation of pure **Ce-MOF** for all three investigated carboxylate precursors—$Ce_6O_8(piv)_8(deta)_4$, $Ce_2(ac)_6(H_2O)_3$, and $Ce_4(OH)_2(piv)_{10}(H_2O)_2$ (Figure 4). Notably, synthesis from $Ce_6O_8(piv)_8(deta)_4$ is accompanied by full reduction of Ce^{4+} to Ce^{3+} due to amine excess.

Variation of $(CH_3)_2NH$ content demonstrated that **Ce-MOF** could be obtained in pure form within a wide range of $(CH_3)_2NH$ content (1 to 10 equiv with respect to Ce), indicating the stability of the framework. Notably, if a simple and commercially available Ce source $Ce(NO_3)_3(H_2O)_6$ was used as a precursor, it was not possible to obtain pure **Ce-MOF** (Figure S5), highlighting the importance of preorganized Ce atom arrangement in the carboxylate precursors for the synthesis. Despite the identical composition of the **Ce-MOF** powders derived from three different precursors, BET surface area measurements clearly indicate a substantial difference in specific surface area of the sample prepared from $Ce_4(OH)_2(piv)_{10}(H_2O)_2$ having S_{BET} (222 m^2/g) twice as large as that of the ones prepared from $Ce_6O_8(piv)_8(deta)_4$ (110 m^2/g) and $Ce_2(ac)_6(H_2O)_3$ (112 m^2/g) (Scheme 1 and Figures S6 and S7).

This can originate from a rather loose arrangement of 1D polymeric structural entities in $Ce_4(OH)_2(piv)_{10}(H_2O)_2$ due

https://doi.org/10.1021/acsomega.3c07906
ACS Omega 2023, 8, 48394−48404

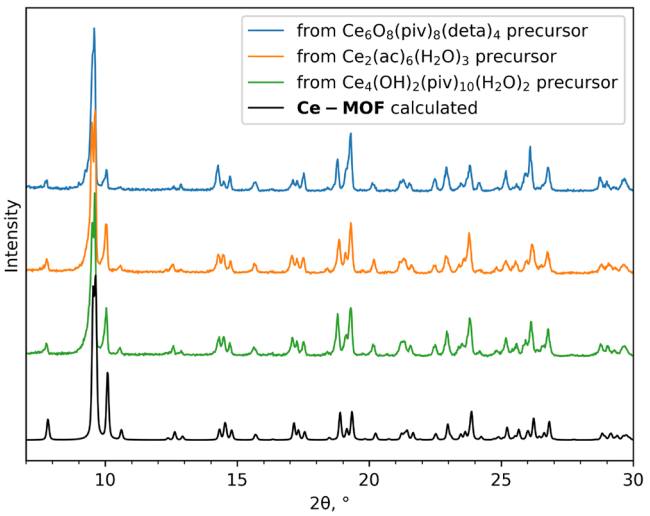

Figure 4. PXRD patterns (λ = 1.5419 Å) of **Ce-MOF** samples prepared from various Ce precursors.

to the bulky pivalate ligands or from a different reactivity of the precursors but requires further investigation. Thus, to the best of our knowledge, **Ce-MOF** having S_{BET} of 222 m^2/g shares the second highest reported specific surface area value among Ce^{3+} MOFs with dicarboxylic linkers.[60,71]

3.4. Crystal Structures of Ce-MOF and Ce-MOF$^{-H_2O}$. **Ce-MOF** crystallizes in the $P2_1/n$ space group, the unit cell contains one symmetrically independent Ce1 atom, and the crystal structure is composed of the centrosymmetric dinuclear $[Ce_2(bdc)_4]^{2-}$ species (Ce1−Ce1^{i} separation equals 4.185 Å) linked by two bridging and two chelate bridging carboxylic groups of four terephthalate anions (bdc^{2-}) (Figure 5 and Figure S8). Each Ce1 is coordinated by O1 and O2 atoms of a chelating bdc^{2-} ion, O3 and O4 atoms of a chelating bridging bdc^{2-}, O5 and O6 atoms of a bridging bdc^{2-}, O3 from another chelating bridging bdc^{2-}, O7 atom from a terminal bdc^{2-}, and O1S from the coordinated DMF molecule. The ninefold coordination environment of Ce1 is best described as a muffin according to CShM (continuous shape measures) analysis (Figure S9 and Table S4).[76] It is worth noting that the geometry of dinuclear $[Ce_2(bdc)_4]^{2-}$ species is typical for cerium carboxylates and, for instance, occurs in $Ce_2(bdc)_3(DMF)_2(DMSO)_2$[48] and $Ce_2(bdc)_2(NMP)_4(ac)_2$[50] MOF structures. However, the presence of a terminal COO group is quite unusual and is due to the formation of ion pairs with $[(CH_3)_2NH_2]^+$ cations. The dinuclear $[Ce_2(bdc)_4]^{2-}$ fragments are joined together into a three-dimensional anionic framework $[Ce_2(bdc)_4]^{2-}_{\infty}$ by the dicarboxylate terephthalate anions of two types, which are considered as μ_2 and μ_4 connectors (Figure 6).

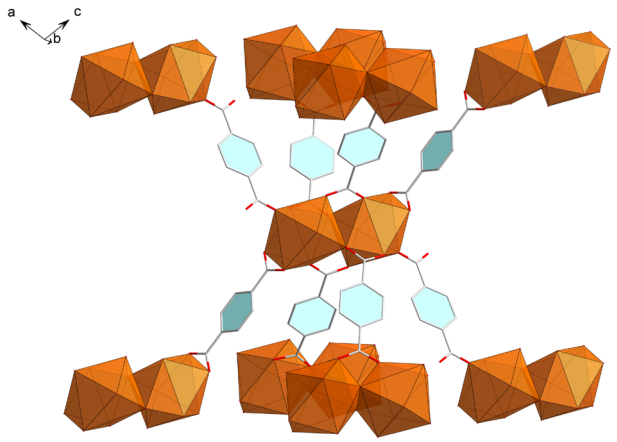

Figure 6. Dinuclear building unit of **Ce-MOF** surrounded by eight neighbor units as a node of an 8-c topological **bcu** net.

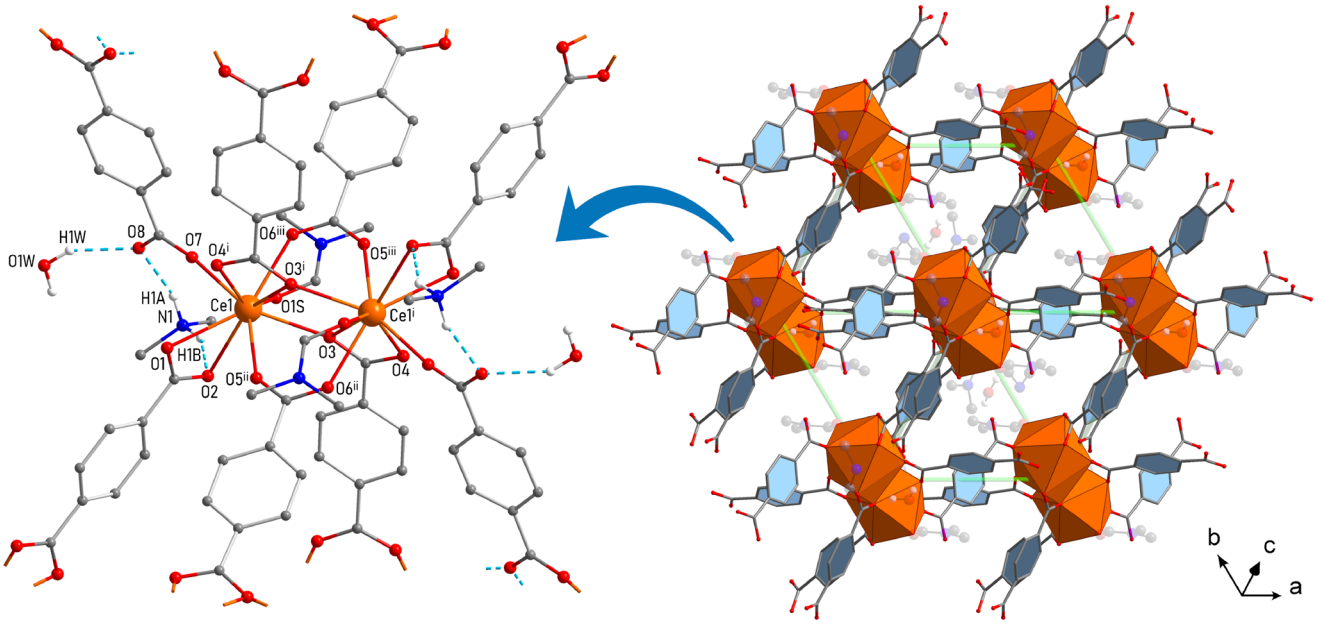

Figure 5. Crystal structure of **Ce-MOF**. The dinuclear building unit on the left is presented as a ball-and-stick model for clarity; see the SI for the thermal ellipsoid plot of the building unit. Dashed lines show H-bonds. Symmetry codes: (i) 1−x, 1−y, 1−z; (ii) 1.5−x, 0.5+y, 1.5−z; (iii) −0.5+x, 0.5−y, −0.5+z. Guest molecules on the right are shown as semitransparent for clarity. The right panel shows the view along the channels in the $[\bar{1}11]$ direction. Semitransparent green lines show unit cell edges.

https://doi.org/10.1021/acsomega.3c07906
ACS Omega 2023, 8, 48394−48404

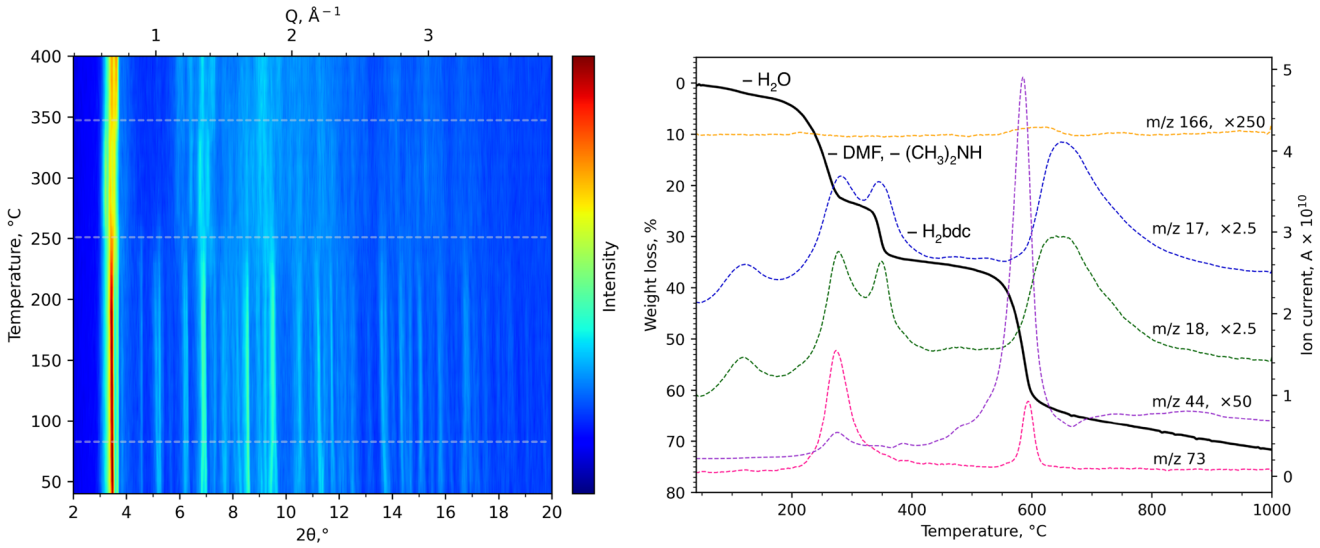

Figure 7. *In situ* PXRD pattern (λ = 0.5594 Å) of **Ce-MOF** upon heating in a capillary sealed in vacuum (left). Semitransparent dashed lines divide the temperature range into several stages of the sample evolution. TG curve of **Ce-MOF** in argon with scaled ionic currents of ions in evolved gas with the respective m/z (right).

The framework features a complex intertwined channel system along the $[1\bar{1}1]$ and $[\bar{1}11]$ directions with the largest rhombic aperture of 9.47 Å × 17.58 Å along the diagonals, as calculated from the distances between Ce ions (Figure 5 and Figure S10). Topology analysis of the **Ce-MOF** crystal structure with ToposPro software[77] indicates that the structure can be represented as an 8-c net (point symbol $\{4.^{24}6^4\}$) of a **bcu**-type topology with Ce_2 building units as nodes (Figure 6 and Figure S11). Porosity analysis of the crystal structure demonstrates the highest porosity of **Ce-MOF** among the reported Ce^{3+}-based MOFs with a terephthalic linker and the third highest porosity after virtual solvent exclusion (Table 1).

Structural analysis of dehydrated **Ce-MOF**$^{-H_2O}$ demonstrates that removal of water molecules does not affect the crystal structure of the framework substantially (Tables S1 and S2) due to its rigidity and only leads to disorder of dimethylammonium cations and dimethylformamide molecules. Porosity analysis of the crystal structure demonstrates the highest porosity of **Ce-MOF** among the reported Ce^{3+}-based MOFs with the terephthalic linker and the third highest porosity after virtual solvent exclusion (Table 1).

Crystal structures of **Ce-MOF** and **Ce-MOF**$^{-H_2O}$ were also determined at room temperature and were demonstrated to have no noticeable differences from the ones at 100 K (Tables S1 and S2). Figure S12 shows the Rietveld refined powder XRD profile of **Ce-MOF**.

3.5. Thermal Behavior. Since MOFs synthesized under solvothermal conditions usually contain guest solvent molecules in the voids, their desolvation upon heating at moderate temperatures is required to activate the porosity. The thermal behavior of the new **Ce-MOF** was investigated by means of *in situ* PXRD, TG-DTA with mass spectrometric evolved gas analysis, and total X-ray scattering with PDF analysis. In the process of thermal decomposition of **Ce-MOF**, several stages can be distinguished. The decomposition begins from the elimination of the weakly bound water molecules (m/z = 18, 17) from the pores at 50−100 °C, the experimental weight loss is 3.1%, which is consistent with the theoretically calculated weight loss of 3.0% (Figure 7 and Figure S13). Judging by the data obtained in the *in situ* PXRD experiment (Figure 7 and Figure S14), only slight structural changes occur (at Q of ca. 1.4 and 1.8 Å^{-1}) with most of the peaks retaining their positions and intensity. This is in line with the SC XRD crystal structure of a **Ce-MOF**$^{-H_2O}$.

Upon further heating, DMF and dimethylamine molecules leave the pores on the next stage of weight loss at 250−275 °C (exp. 22.8%, calcd 22.4%) and appearance of peaks in the mass spectrum with m/z = 73 (DMF^+), 44 ($((CH_3)_2N^+$), 18 (NH_4^+), 17 (NH_3^+). This corresponds to the major change in PXRD pattern (see detailed view in Figures S15 and S16) manifested in intensity drop and disappearance of several diffraction peaks (e.g., at 0.8−1 Å^{-1}). Lighter dimethylamine molecules residing in the pores of the framework are eliminated simultaneously with the heavier coordinated dimethylformamide molecules due to the firm retention in the form of $(CH_3)_2NH_2^+$ cations by the anionic framework $[Ce_2(bdc)_4]^{2-}$ and a system of H-bonds. The proton that should remain upon elimination of dimethylamine for charge compensation is supposedly bound to the O8 atom of the terminal bdc^{2-} ligand that acted as the H-bond acceptor from $(CH_3)_2NH_2^+$ in the as-obtained **Ce-MOF**.

At ca. 350 °C, one H_2bdc molecule per formula unit is eliminated, leaving the $Ce_2(bdc)_3$ framework (exp. and calcd weight losses of 36.0%). According to TG-DTA-MS data, the framework exhibits thermal stability up to at least 450 °C in argon while the peaks of m/z 44, 73, and 166 at higher temperatures originate from terephthalic linkers indicating MOF destruction. The argon atmosphere impedes oxidation, and the formation of CeO_2 is only achieved by 1000 °C (exp. and calcd weight losses of 72.0 and 71.6%, respectively). The thermal behavior of **Ce-MOF** in air demonstrates the same three elimination stages at temperatures of 100−150, 200−250, and 300−350 °C while combustion of the framework occurs in the temperature range of 390−500 °C with the formation of CeO_2 (Figure S17).

To get more insight into the structural changes in **Ce-MOF** upon heating, we performed total scattering experiments with PDF analysis of as-synthesized **Ce-MOF** and of the products of its heating at 100 (**Ce-MOF**$^{-H_2O}$), 250 ($[Ce_2(bdc)_3(H_2bdc)]$), and 400 °C ($[Ce_2(bdc)_3]$) in a vacuum (Figure 8). The data

https://doi.org/10.1021/acsomega.3c07906
ACS Omega 2023, 8, 48394−48404

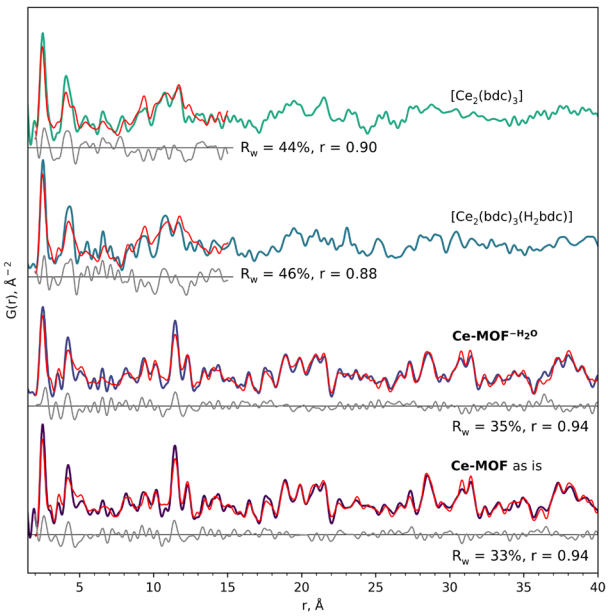

Figure 8. Measured PDF data (shades of blue) of **Ce-MOF** samples (as is and heated to different temperatures) and refinements (red) with the corresponding periodic models. Difference curves (gray) are offset for clarity. Weighted residual factor R_w and Pearson correlation coefficient r between experimental and fitted curves are shown below the graphs.

were collected according to our previously developed procedure.[78] See the Supporting Information for the details on data collection and choice of structure models for the refinements.

The PDFs of **Ce-MOF** and **Ce-MOF**$^{-H_2O}$ closely resemble each other, which is reflected in their Pearson correlation coefficient r value of 0.98 (Figure S18) and are well described by the corresponding structure models of **Ce-MOF** and **Ce-MOF**$^{-H_2O}$ within a distance range of up to 40 Å, which indicates that the local structure remains unchanged upon elimination of water molecules.

Heating of **Ce-MOF** up to 250 °C is accompanied by departure of DMF and dimethylamine molecules and leads to formation of $[Ce_2(bdc)_3(H_2bdc)]$, and a substantial change of the structure is expressed in both *in situ* PXRD and PDF data (Figures 7 and 8, respectively). The local structure changes and the peaks corresponding to Ce−Ce distances (e.g., at 11.4 and 28.4 Å) become less pronounced in the PDF of $[Ce_2(bdc)_3(H_2bdc)]$ indicating partial loss of the long-range order. PDF of $[Ce_2(bdc)_3]$ is similar to the one of $[Ce_2(bdc)_3(H_2bdc)]$ with an r value of 0.91.

Due to the change of structure between 100 and 250 °C, the last two PDFs differ significantly from the first two, which is quantitatively expressed in the Pearson correlation coefficient values of ca. 0.7 (Figure S17). At the same time, the two PDFs are fitted rather well with the $Ce_5(bdc)_{7.5}$ model constructed from the $Ce_5(bdc)_{7.5}(DMF)_4$ crystal structure[31] by exclusion of DMF within the short distance range up to 15 Å, which points to substantial structure change upon elimination of DMF and dimethylamine and only a minor change between 250 and 400 °C.

PXRD patterns of **Ce-MOF** above 350 °C (Figure 7), a previously reported product of **Ce5** heating above 275 °C in the N_2 atmosphere,[71] and that of CeO_2**@Ce5** above 275 °C (Figure S19) are similar to each other, and these three substances contain the same modification of $Ce_2(bdc)_3$. It should be noted that poor crystallinity of that phase hinders the structural study by means of Rietveld refinement; therefore, its crystal structure remains to be determined.

In an oxidizing atmosphere, $Ce_2(bdc)_3$ is readily oxidized to form nano ceria (Figures S15). The oxidation process depends on the surface area of the initial MOF and thus on the precursor employed. The largest surface area of **Ce-MOF** is obtained in the case of the $Ce_4(OH)_2(piv)_{10}(H_2O)_2$ precursor (222 m^2/g) and the corresponding **Ce-MOF** is fully oxidized to CeO_2 at 390 °C, while the **Ce-MOF** sample synthesized from $Ce_2(ac)_6(H_2O)_3$ only forms traces of CeO_2 at that temperature and full combustion occurs after heating at a constant temperature of 400 °C for 10 min (Figure S20).

Here, we have also studied the CeO_2**@Ce5** composite behavior upon heating in a vacuum (Figure S19). It has been found that nanoceria does not influence thermal decomposition of the **Ce5** framework in composite, which loses DMF at 250 °C and undergoes pyrolysis after 475°C similarly to pure **Ce5**, while nanoceria gradually crystallizes upon heating.

3.6. Catalytic Performance of MOF-Derived CeO_2. MOFs are widely explored as catalysts for various industrially important processes with the Ce-based ones and their derivatives, e.g., MOF-derived ceria being the most prominent in redox reactions due to the two stable oxidation states of Ce.[33−36] Many reports point to the high catalytic activity of CeO_2 and its composites in the CO oxidation reaction:[38,39,79,80]

$$CO + 0.5O_2 \rightarrow CO_2$$

Less attention was devoted to Ce-based MOFs with only several reported examples indicating high efficiency of these MOFs and corresponding composites.[81,82]

Preliminary catalytic experiments demonstrated that no activity is exhibited by **Ce-MOF** and **Ce5** per se at lower temperatures and the activation to form the MOF-derived CeO_2 is essential. The **Ce-MOF** sample with the lowest surface area (112 m^2/g) prepared from the $Ce_2(ac)_6(H_2O)_3$ precursor did not oxidize to CeO_2 under the conditions of the catalytic reaction even at 400°C but transformed to $[Ce_2(bdc)_3]$ and thus did not exhibit catalytic activity (Figure 9, Figure S21, and Table S5). At the same time, all other MOFs that transformed to CeO_2 *in situ* demonstrate comparable activity with the conversion of CO at the level of ca. 30% corresponding to the 16 mmol h^{-1} g^{-1} reaction rate, which is significantly higher than that of bulk CeO_2 (Figure 9). A minor decrease of activity of derived CeO_2 from **Ce5**, CeO_2**@Ce5**, and **Ce-MOF** is in perfect correlation with the decrease of the CeO_2 BET surface area: 224, 188, and 182 m^2/g, respectively (Table S5). The only reaction product is CO_2; accordingly, the selectivity for CO_2 is 100%. The material balance of the reaction for carbon calculated from gas chromatography data is 95−98% (Figure S22 and Table S6).

Further studies of the activity and life cycle of the catalyst were performed for **Ce-MOF**. Since only around 30% conversion of CO was achieved during the preliminary experiments, the loading mass of the catalyst was increased, keeping all other reaction conditions unchanged. The efficiency of the catalyst increases significantly upon *in situ* transformation to CeO_2 at ca. 350°C on the first cycle (Figure 10), and high CO conversion (80%) is already observed at a temperature of 270 °C on the second cycle. The lifetime of the catalyst was examined, and it demonstrated to maintain its high

https://doi.org/10.1021/acsomega.3c07906
ACS Omega 2023, 8, 48394−48404

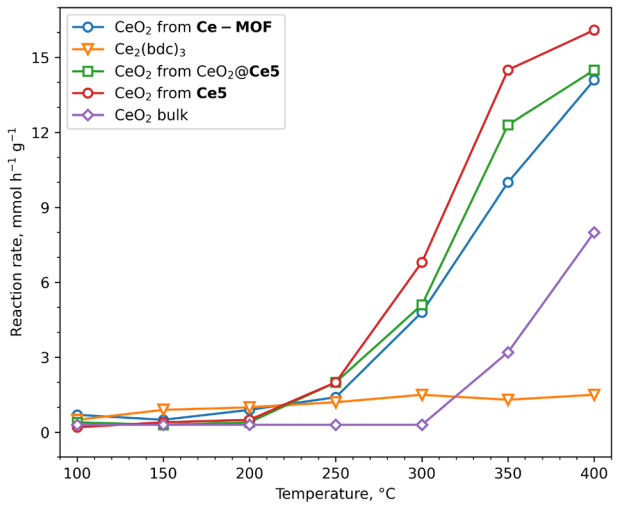

Figure 9. Reaction rate of CO oxidation on catalysts *in situ* derived from **Ce-MOF**, **Ce5**, and CeO_2**@Ce5** per gram of loading. $Ce_2(bdc)_3$ is formed from **Ce-MOF** (S_{BET} = 112 m^2/g) synthesized from the $Ce_2(ac)_6(H_2O)_3$ precursor, while **Ce-MOF** (S_{BET} = 222 m^2/g) synthesized from the $Ce_4(OH)_2(piv)_{10}(H_2O)_2$ precursor forms CeO_2. The reaction rate on bulk crystalline CeO_2 is provided for reference. CO:air ratio is 1:4; gas flow is 20 mL/min. Loading mass 0.2 g of sample +0.3 g of quartz.

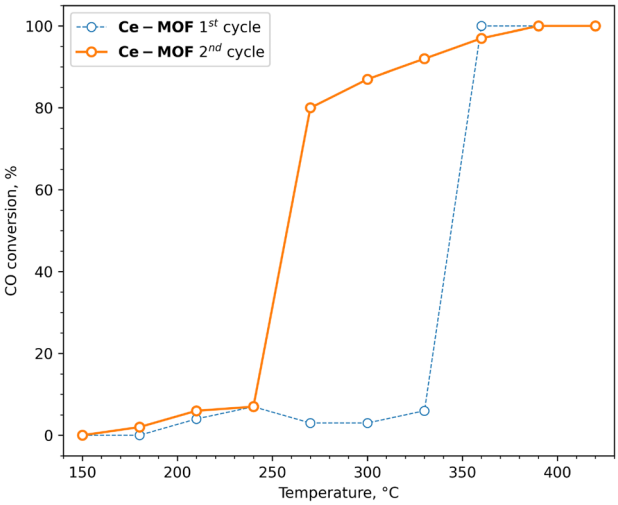

Figure 10. Activity of the catalyst in the CO oxidation reaction. The CO:air ratio is 1:4; the gas flow is 20 mL/min. Loading mass of **Ce-MOF** 0.4 g. 1st cycle (blue line) corresponds to *in situ* combustion of the loaded **Ce-MOF** to CeO_2 under the conditions of the catalytic reaction; 2nd cycle (orange line) corresponds to the activity of CeO_2 derived from **Ce-MOF** for the whole examined temperature range.

efficiency for more than 14 h at 300 °C (Figure S23). The catalytic activity of the **Ce-MOF**-derived CeO_2 is comparable to the reported catalysts in CO oxidation (Table S7).[38,39,79,81,82]

4. CONCLUSIONS

To conclude, the novel Ce^{3+}-based MOF $[(CH_3)_2NH_2]_2[Ce_2(bdc)_4(DMF)_2]\cdot 2H_2O$ (**Ce-MOF**) has been prepared by solvothermal reaction in DMF from various Ce carboxylates with terephthalic acid (H_2bdc) and dimethylamine. The choice of carboxylate precursor did not impact the phase composition; however, it affected the specific surface area of the obtained material. In the absence of added dimethylamine, the solvothermal reaction leads to the formation of $Ce_5(bdc)_{7.5}(DMF)_4$ (**Ce5**) or its composite CeO_2**@Ce5**. It is worth noting that while nano-CeO_2 is hardly visible in PXRD patterns of the composite, its signal dominates the PDF. This highlights the value of total scattering for characterization of the MOFs that could contain amorphous or nanocrystalline admixtures.

Ce-MOF has 3D connectivity of the **bcu** type with a dinuclear fragment connected with eight neighbors and three types of solvate species residing in its pores: water, DMF, and dimethylammonium cation.

The framework retains its integrity upon elimination of water molecules, while departure of DMF and dimethylamine leads to substantial structural transformation, which was evidenced through *in situ* XRD, thermogravimetric analysis, and total scattering experiments with PDF analysis.

Further heating leads to formation of $Ce_2(bdc)_3$, which is stable up to at least 450 °C in nonoxidative conditions and undergoes combustion after 390 °C to form nano-CeO_2. MOF-derived CeO_2 has a mean crystallite size of ca. 5−6 nm and exhibits catalytic activity in the CO oxidation reaction.

Finally, we developed a synthetic strategy for a new anionic Ce-based MOF formed due to the templating effect of deliberately added dimethylamine. We believe that the proposed approach could pave the way for the synthesis of new anionic MOFs.

■ ASSOCIATED CONTENT

Supporting Information

The Supporting Information is available free of charge at https://pubs.acs.org/doi/10.1021/acsomega.3c07906.

Crystal structure and refinement data (ZIP)

Experimental section; synthesis; X-ray crystallography; thermal behavior; and catalytic performance (PDF)

Accession Codes

CCDC 2106041−2106042, 2238303−2238304 contain the supplementary crystallographic data for this paper. These data can be obtained free of charge via www.ccdc.cam.ac.uk/data_request/cif, or by emailing data_request@ccdc.cam.ac.uk, or by contacting The Cambridge Crystallographic Data Centre, 12 Union Road, Cambridge CB2 1EZ, UK; fax: + 44 1223 336033

■ AUTHOR INFORMATION

Corresponding Author

Dmitry Tsymbarenko − *Lomonosov Moscow State University, Moscow 119991, Russia;* orcid.org/0000-0002-2818-5639; Email: tsymbarenko@inorg.chem.msu.ru

Authors

Dimitry Grebenyuk − *Lomonosov Moscow State University, Moscow 119991, Russia; Faculty of Materials Science, MSU-BIT University, Shenzhen 518172, China;* orcid.org/0000-0002-4723-8564

Maria Shaulskaya − *Lomonosov Moscow State University, Moscow 119991, Russia;* orcid.org/0000-0002-0340-9157

Artem Shevchenko − *Max Planck Institute for Solid State Research, Stuttgart 70569, Germany; Lomonosov Moscow State University, Moscow 119991, Russia;* Present Address: Max Planck Institute for Solid State Research,

https://doi.org/10.1021/acsomega.3c07906
ACS Omega 2023, 8, 48394−48404

Stuttgart 70569, Germany; orcid.org/0000-0001-8378-1022

Mirijam Zobel − *Institute of Crystallography, RWTH Aachen University, Aachen 52066, Germany;* orcid.org/0000-0002-8207-8316

Marina Tedeeva − *Lomonosov Moscow State University, Moscow 119991, Russia;* orcid.org/0000-0002-4929-5853

Alexander Kustov − *Lomonosov Moscow State University, Moscow 119991, Russia; N. D. Zelinsky Institute of Organic Chemistry, Russian Academy of Sciences, Moscow 119991, Russia;* orcid.org/0000-0003-0869-8784

Ilia Sadykov − *Paul Scherrer Institute, Villigen 5232, Switzerland;* orcid.org/0000-0003-1549-4771

Complete contact information is available at: https://pubs.acs.org/10.1021/acsomega.3c07906

Author Contributions

D.T. conceived the idea, secured funding, and supervised the project. D.G. and M.S. synthesized and characterized the compounds. M.Z. enabled access to lab diffractometer for PDF data collection, provided expertise in the field, and contributed to the data analysis and discussion. D.T. and D.G. collected single-crystal and powder diffraction data and solved and refined the crystal structures. A.S., D.G., and D.T. performed the *in situ* PXRD experiments. A.K. and M.T. measured the nitrogen adsorption isotherms and performed catalytic activity studies. I.S. measured and interpreted XANES spectra. D.G. took the lead in writing of the manuscript with contributions from D.T., M.Z., and A.K. All authors have given approval to the final version of the manuscript.

Funding

D.G., M.S., M.T., and D.T. acknowledge the support by RSF (project no. 22-73-10089). Diffraction data collection at Elettra synchrotron was partially funded by the CALIPSOplus project from the EU Framework Programme for Research and Innovation HORIZON 2020 (Grant Agreement 730872). A.S. acknowledges the DFG-Grant BE 7407/1-1 for partial funding of *in situ* PXRD data collection in an inert atmosphere.

Notes

The authors declare no competing financial interest.

■ ACKNOWLEDGMENTS

D.T. and D.G. acknowledge the Elettra synchrotron facility (XRD1 and MCX beamlines, Trieste, Italy) and the Kurchatov synchrotron radiation source (Belok/XSA beamline, Moscow, Russia) for the awarded beamtime. The valuable support from Dr. Maurizio Polentarutti, Dr. Giorgio Bais, Dr. Jasper Plaisier, and Dr. Roman Svetogorov during powder and single-crystal XRD experiments is gratefully acknowledged. A.S. is very thankful to Dr. Sebastian Bette (Institute for Solid State Research, Stuttgart, Germany) for his help in PXRD experiments. M.T. and A.K. thank Dr. Gennady Kapustin from the Institute of Organic Chemistry for surface area measurements. D.T. acknowledges the support from the M.V. Lomonosov Moscow State University Program of Development.

■ REFERENCES

(1) Morris, R. E.; Wheatley, P. S. Gas Storage in Nanoporous Materials. *Angew. Chem., Int. Ed.* **2008**, *47* (27), 4966−4981.

(2) Li, H.; Wang, K.; Sun, Y.; Lollar, C. T.; Li, J.; Zhou, H.-C. Recent Advances in Gas Storage and Separation Using Metal−Organic Frameworks. *Mater. Today* **2018**, *21* (2), 108−121.

(3) Lee, C. Y.; Bae, Y.-S.; Jeong, N. C.; Farha, O. K.; Sarjeant, A. A.; Stern, C. L.; Nickias, P.; Snurr, R. Q.; Hupp, J. T.; Nguyen, S. T. Kinetic Separation of Propene and Propane in Metal−Organic Frameworks: Controlling Diffusion Rates in Plate-Shaped Crystals via Tuning of Pore Apertures and Crystallite Aspect Ratios. *J. Am. Chem. Soc.* **2011**, *133* (14), 5228−5231.

(4) Huangfu, M.; Wang, M.; Lin, C.; Wang, J.; Wu, P. Luminescent Metal−Organic Frameworks as Chemical Sensors Based on "Mechanism−Response": A Review. *Dalton Trans.* **2021**, *50* (10), 3429−3449.

(5) Fang, X.; Zong, B.; Mao, S. Metal−Organic Framework-Based Sensors for Environmental Contaminant Sensing. *Nano-Micro Lett.* **2018**, *10* (4), 64.

(6) Liu, C.-Y.; Chen, X.-R.; Chen, H.-X.; Niu, Z.; Hirao, H.; Braunstein, P.; Lang, J.-P. Ultrafast Luminescent Light-Up Guest Detection Based on the Lock of the Host Molecular Vibration. *J. Am. Chem. Soc.* **2020**, *142* (14), 6690−6697.

(7) Yu, C.-X.; Hu, F.-L.; Song, J.-G.; Zhang, J.-L.; Liu, S.-S.; Wang, B.-X.; Meng, H.; Liu, L.-L.; Ma, L.-F. Ultrathin Two-Dimensional Metal-Organic Framework Nanosheets Decorated with Tetra-Pyridyl Calix[4]Arene: Design, Synthesis and Application in Pesticide Detection. *Sens. Actuators, B* **2020**, *310*, No. 127819.

(8) Zhang, C.; Qin, Y.; Ke, Z.; Yin, L.; Xiao, Y.; Zhang, S. Highly Efficient and Facile Removal of As(V) from Water by Using Pb-MOF with Higher Stable and Fluorescence. *Appl. Organomet. Chem.* **2023**, *37* (5), No. e7066.

(9) Chen, Y.; Chen, Z.; Yuan, L.; Xiao, Y.; Zhang, S.-H.; Li, N. Adsorption of PO43-, Cd(II), Pb(II), Cu(II), As(III), and As(V) Using a Carbonised Mn-Based Metal−Organic Framework. *Arabian Journal of Chemistry* **2023**, *16* (8), No. 104950.

(10) Wu, M.-X.; Yang, Y.-W. Metal−Organic Framework (MOF)-Based Drug/Cargo Delivery and Cancer Therapy. *Adv. Mater.* **2017**, *29* (23), 1606134.

(11) Kotzabasaki, M.; Froudakis, G. E. Review of Computer Simulations on Anti-Cancer Drug Delivery in MOFs. *Inorg. Chem. Front.* **2018**, *5* (6), 1255−1272.

(12) Liu, J.; Chen, L.; Cui, H.; Zhang, J.; Zhang, L.; Su, C.-Y. Applications of Metal−Organic Frameworks in Heterogeneous Supramolecular Catalysis. *Chem. Soc. Rev.* **2014**, *43* (16), 6011−6061.

(13) Al-Rowaili, F. N.; Jamal, A.; Ba Shammakh, M. S.; Rana, A. A Review on Recent Advances for Electrochemical Reduction of Carbon Dioxide to Methanol Using Metal−Organic Framework (MOF) and Non-MOF Catalysts: Challenges and Future Prospects. *ACS Sustainable Chem. Eng.* **2018**, *6* (12), 15895−15914.

(14) Goetjen, T. A.; Liu, J.; Wu, Y.; Sui, J.; Zhang, X.; Hupp, J. T.; Farha, O. K. Metal−Organic Framework (MOF) Materials as Polymerization Catalysts: A Review and Recent Advances. *Chem. Commun.* **2020**, *56* (72), 10409−10418.

(15) Pang, J.; Jiang, T.; Ke, Z.; Xiao, Y.; Li, W.; Zhang, S.; Guo, P. Wood Cellulose Nanofibers Grafted with Poly(ε-Caprolactone) Catalyzed by ZnEu-MOF for Functionalization and Surface Modification of PCL Films. *Nanomaterials* **2023**, *13* (13), 1904.

(16) Pang, J.; Gao, Q.; Yin, L.; Zhang, S. Synthesis and Catalytic Performance of Banana Cellulose Nanofibres Grafted with Poly(ε-Caprolactone) in a Novel Two-Dimensional Zinc(II) Metal-Organic Framework. *Int. J. Biol. Macromol.* **2023**, *224*, 568−577.

(17) Guo, P.; Zhang, S.; Cheng, H.; Zeng, X.; Wang, H.; Fischer, R. A.; Muhler, M. Significantly Boosted Activity for Styrene Oxidation through Simultaneous Regulation of Porosity and Copper Sites in Microporous Metal−Organic Framework Cu-BTC. *Catal. Sci. Technol.* **2023**, *13* (9), 2728−2734.

(18) Gao, Q.-F.; Jiang, T.-L.; Li, W.-Z.; Tan, D.-F.; Zhang, X.-H.; Pang, J.-Y.; Zhang, S.-H. Porous and Stable Zn-Series Metal−Organic Frameworks as Efficient Catalysts for Grafting Wood Nanofibers with Polycaprolactone via a Copolymerization Approach. *Inorg. Chem.* **2023**, *62* (8), 3464−3473.

(19) Wang, M.-F.; Mi, Y.; Hu, F.-L.; Hirao, H.; Niu, Z.; Braunstein, P.; Lang, J.-P. Controllable Multiple-Step Configuration Transformations in a Thermal/Photoinduced Reaction. *Nat. Commun.* **2022**, *13* (1), 2847.
(20) Wang, M.-F.; Mi, Y.; Hu, F.-L.; Niu, Z.; Yin, X.-H.; Huang, Q.; Wang, H.-F.; Lang, J.-P. Coordination-Driven Stereospecific Control Strategy for Pure Cycloisomers in Solid-State Diene Photocycloaddition. *J. Am. Chem. Soc.* **2020**, *142* (2), 700−704.
(21) Li, F.-L.; Shao, Q.; Huang, X.; Lang, J.-P. Nanoscale Trimetallic Metal-Organic Frameworks Enable Efficient Oxygen Evolution Electrocatalysis. *Angew. Chem., Int. Ed.* **2018**, *57* (7), 1888−1892.
(22) Li, F.; Wang, P.; Huang, X.; Young, D. J.; Wang, H.; Braunstein, P.; Lang, J. Large-Scale, Bottom-Up Synthesis of Binary Metal−Organic Framework Nanosheets for Efficient Water Oxidation. *Angew. Chem., Int. Ed.* **2019**, *58* (21), 7051−7056.
(23) Rosi, N. L.; Eckert, J.; Eddaoudi, M.; Vodak, D.; Kim, J.; O'Keeffe, M.; Yaghi, O. M. Hydrogen Storage in Microporous Metal-Organic Frameworks. *Science* **2003**, *300* (5622), 1127−1129.
(24) Millange, F.; Serre, C.; Férey, G. Synthesis, Structure Determination and Properties of MIL-53as and MIL-53ht: The First Criii Hybrid Inorganic−Organic Microporous Solids: Criii(OH)·{O2C−C6H4−CO2}·{HO2C−C6H4−CO2H}x. *Chem. Commun.* **2002**, *8*, 822−823.
(25) Cavka, J. H.; Jakobsen, S.; Olsbye, U.; Guillou, N.; Lamberti, C.; Bordiga, S.; Lillerud, K. P. A New Zirconium Inorganic Building Brick Forming Metal Organic Frameworks with Exceptional Stability. *J. Am. Chem. Soc.* **2008**, *130* (42), 13850−13851.
(26) Cui, Y.; Yue, Y.; Qian, G.; Chen, B. Luminescent Functional Metal−Organic Frameworks. *Chem. Rev.* **2012**, *112* (2), 1126−1162.
(27) Zhao, S. N.; Wang, G.; Poelman, D.; Voort, P. Luminescent Lanthanide MOFs: A Unique Platform for Chemical Sensing. *Materials* **2018**, *11* (4), 572.
(28) Li, B.; Wen, H. M.; Cui, Y.; Zhou, W.; Qian, G.; Chen, B. Emerging Multifunctional Metal−Organic Framework Materials. *Adv. Mater.* **2016**, *28* (40), 8819−8860.
(29) Moosavi, S. M.; Nandy, A.; Jablonka, K. M.; Ongari, D.; Janet, J. P.; Boyd, P. G.; Lee, Y.; Smit, B.; Kulik, H. J. Understanding the Diversity of the Metal-Organic Framework Ecosystem. *Nat. Commun.* **2020**, *11* (1), 4068.
(30) Han, Y.; Li, X.; Li, L.; Ma, C.; Shen, Z.; Song, Y.; You, X. Structures and Properties of Porous Coordination Polymers Based on Lanthanide Carboxylate Building Units. *Inorg. Chem.* **2010**, *49* (23), 10781−10787.
(31) D'Arras, L.; Sassoye, C.; Rozes, L.; Sanchez, C.; Marrot, J.; Marre, S.; Aymonier, C. Fast and Continuous Processing of a New Sub-Micronic Lanthanide-Based Metal-Organic Framework. *New J. Chem.* **2014**, *38* (4), 1477−1483.
(32) Vizuet, J. P.; Lewis, A. L.; Mccandless, G. T.; Balkus, K. J. Holmium-Based Metal-Organic Frameworks Using the BDC Linker. *Polyhedron* **2021**, *205*, No. 115283.
(33) Zhu, C.; Ding, T.; Gao, W.; Ma, K.; Tian, Y.; Li, X. CuO/CeO2 Catalysts Synthesized from Ce-UiO-66 Metal-Organic Framework for Preferential CO Oxidation. *Int. J. Hydrogen Energy* **2017**, *42* (27), 17457−17465.
(34) Campanelli, M.; Del Giacco, T.; De Angelis, F.; Mosconi, E.; Taddei, M.; Marmottini, F.; D'Amato, R.; Costantino, F. Solvent-Free Synthetic Route for Cerium(IV) Metal−Organic Frameworks with UiO-66 Architecture and Their Photocatalytic Applications. *ACS Appl. Mater. Interfaces* **2019**, *11* (48), 45031−45037.
(35) Lammert, M.; Wharmby, M. T.; Smolders, S.; Bueken, B.; Lieb, A.; Lomachenko, K. A.; Vos, D. D.; Stock, N. Cerium-Based Metal Organic Frameworks with UiO-66 Architecture: Synthesis, Properties and Redox Catalytic Activity. *Chem. Commun.* **2015**, *51* (63), 12578−12581.
(36) Peng, M. M.; Ganesh, M.; Vinodh, R.; Palanichamy, M.; Jang, H. T. Solvent Free Oxidation of Ethylbenzene over Ce-BTC MOF. *Arabian Journal of Chemistry* **2019**, *12* (7), 1358−1364.
(37) Smolders, S.; Lomachenko, K. A.; Bueken, B.; Struyf, A.; Bugaev, A. L.; Atzori, C.; Stock, N.; Lamberti, C.; Roeffaers, M. B. J.; De Vos, D. E. Unravelling the Redox-Catalytic Behavior of Ce $^{4+}$ Metal-Organic Frameworks by X-Ray Absorption Spectroscopy. *ChemPhysChem* **2018**, *19* (4), 373−378.
(38) Dey, S.; Dhal, G. C. Cerium Catalysts Applications in Carbon Monoxide Oxidations. *Materials Science for Energy Technologies* **2020**, *3*, 6−24.
(39) He, H.; Yang, P.; Li, J.; Shi, R.; Chen, L.; Zhang, A.; Zhu, Y. Controllable Synthesis, Characterization, and CO Oxidation Activity of CeO 2 Nanostructures with Various Morphologies. *Ceram. Int.* **2016**, *42* (6), 7810−7818.
(40) Jacobsen, J.; Ienco, A.; D'Amato, R.; Costantino, F.; Stock, N. The chemistry of Ce-Based Metal-Organic Frameworks. *Dalton Trans.* **2020**, 16551 DOI: 10.1039/d0dt02813d.
(41) Lammert, M.; Wharmby, M. T.; Smolders, S.; Bueken, B.; Lieb, A.; Lomachenko, K. A.; Vos, D. D. De; Stock, N. UiO-66 Architecture: Synthesis, Properties and Redox Catalytic Activity †. *Chem. Commun.* **2015**, *51* (63), 12578−12581.
(42) Liu, K.; You, H.; Jia, G.; Zheng, Y.; Huang, Y.; Song, Y.; Yang, M.; Zhang, L.; Zhang, H. Hierarchically Nanostructured Coordination Polymer: Facile and Rapid Fabrication and Tunable Morphologies. *Cryst. Growth Des.* **2010**, *10* (2), 790−797.
(43) Gil-Hernández, B.; Maclaren, J. K.; Höppe, H. A.; Pasán, J.; Sanchiz, J.; Janiak, C. Homochiral Lanthanoid(Iii) Mesoxalate Metal−Organic Frameworks: Synthesis, Crystal Growth, Chirality, Magnetic and Luminescent Properties. *CrystEngComm* **2012**, *14* (8), 2635.
(44) Seidel, C.; Lorbeer, C.; Cybińska, J.; Mudring, A.-V.; Ruschewitz, U. Lanthanide Coordination Polymers with Tetrafluoroterephthalate as a Bridging Ligand: Thermal and Optical Properties. *Inorg. Chem.* **2012**, *51* (8), 4679−4688.
(45) Ayhan, O.; Malaestean, I. L.; Ellern, A.; van Leusen, J.; Baca, S. G.; Kögerler, P. Assembly of Cerium(III) 2,2′-Bipyridine-5,5′-Dicarboxylate-Based Metal−Organic Frameworks by Solvent Tuning. *Cryst. Growth Des.* **2014**, *14* (7), 3541−3548.
(46) Speck, A. L. *PLATON, a Multipurpose Crystallographic Tool*, 1980. http://www.platonsoft.nl.
(47) Yu, L.-Q.; Huang, R.-D.; Xu, Y.-Q.; Liu, T.-F.; Chu, W.; Hu, C.-W. Syntheses, Structures and Properties of Novel 3D Lanthanide Metal-Organic Frameworks with Paddle-Wheel Building Blocks. *Inorg. Chim. Acta* **2008**, *361* (7), 2115−2122.
(48) Abbasi, A.; Mohammadnezhad, F.; Geranmayeh, S. A Novel 3-D Nanoporous Ce(III) Metal-Organic Framework with Terephthalic Acid; Thermal, Topology, Porosity and Structural Studies. *J. Inorg. Organomet Polym.* **2014**, *24* (6), 1021−1026.
(49) Zhang, J.; Bu, J. T.; Chen, S.; Wu, T.; Zheng, S.; Chen, Y.; Nieto, R. A.; Feng, P.; Bu, X. Urothermal Synthesis of Crystalline Porous Materials. *Angewandte Chemie - International Edition* **2010**, *49* (47), 8876−8879.
(50) Geranmayeh, S.; Mohammadnezhad, F.; Abbasi, A. Preparation of Ceria Nanoparticles by Thermal Decomposition of a New Two Dimensional Ce(III) Coordination Polymer. *J. Inorg. Organomet Polym.* **2016**, *26* (1), 109−116.
(51) Wang, X.; Wang, Y.; Silver, M. A.; Gui, D.; Bai, Z.; Wang, Y.; Liu, W.; Chen, L.; Diwu, J.; Chai, Z.; Wang, S. Superprotonic Conduction through One-Dimensional Ordered Alkali Metal Ion Chains in a Lanthanide-Organic Framework. *Chem. Commun.* **2018**, *54* (35), 4429−4432.
(52) Nagarkar, S. S.; Unni, S. M.; Sharma, A.; Kurungot, S.; Ghosh, S. K. Two-in-One: Inherent Anhydrous and Water-Assisted High Proton Conduction in a 3D Metal-Organic Framework. *Angew. Chem., Int. Ed.* **2014**, *53* (10), 2638−2642.
(53) Si, X.-J.; Jia, J.; Bao, Y.-L.; Wu, Y.-P.; Liu, Y.; Dong, W.-W.; Zhao, J.; Li, D.-S. Superprotonic Conductivity of a 3D Anionic Metal-Organic Framework by Synergistic Effect of Guest [Me2NH2]+ Cations, Water Molecules and Host Carboxylates. *J. Solid State Chem.* **2021**, *299*, No. 122168.
(54) Wu, B.; Zhang, W.-H.; Ren, Z.-G.; Lang, J.-P. A 1D Anionic Coordination Polymer Showing Superior Congo Red Sorption and Its

https://doi.org/10.1021/acsomega.3c07906
ACS Omega 2023, 8, 48394−48404

Dye Composite Exhibiting Remarkably Enhanced Photocurrent Response. *Chem. Commun.* **2015**, *51* (80), 14893−14896.
(55) Chakraborty, A.; Bhattacharyya, S.; Hazra, A.; Ghosh, A. C.; Maji, T. K. Post-Synthetic Metalation in an Anionic MOF for Efficient Catalytic Activity and Removal of Heavy Metal Ions from Aqueous Solution. *Chem. Commun.* **2016**, *52* (13), 2831−2834.
(56) Boronin, A. I.; Slavinskaya, E. M.; Figueroba, A.; Stadnichenko, A. I.; Kardash, T. Yu.; Stonkus, O. A.; Fedorova, E. A.; Muravev, V. V.; Svetlichnyi, V. A.; Bruix, A.; Neyman, K. M. CO Oxidation Activity of Pt/CeO2 Catalysts below 0 °C: Platinum Loading Effects. *Applied Catalysis B: Environmental* **2021**, *286*, No. 119931.
(57) Grebenyuk, D.; Zobel, M.; Polentarutti, M.; Ungur, L.; Kendin, M.; Zakharov, K.; Degtyarenko, P.; Vasiliev, A.; Tsymbarenko, D. A Family of Lanthanide hydroxo Carboxylates with 1D Polymeric Topology and Ln 4 Butterfly Core Exhibits Switchable Supramolecular Arrangement. *Inorg. Chem.* **2021**, *60* (11), 8049−8061.
(58) Grebenyuk, D.; Martynova, I.; Tsymbarenko, D. Self-Assembly of hexanuclear Lanthanide Carboxylate Clusters of Three Architectures. *Eur. J. Inorg. Chem.* **2019**, *2019*, 3103−3111.
(59) Tsymbarenko, D. M.; Grebenyuk, D. I.; Burlakova, M. A.; Shurkina, A. S. tetranuclear hydroxo Complexes of Rare-Earth Elements with the Cubane Core as Products of Self-Controlled Hydrolysis. *Russ. J. Coord. Chem./Koord. Khimiya* **2022**, *48* (3), 164−172.
(60) Derakhshandeh, P. G.; Abednatanzi, S.; Leus, K.; Janczak, J.; Van Deun, R.; Van Der Voort, P.; Van Hecke, K. Ce(III)-Based Frameworks: From 1D Chain to 3D Porous Metal−Organic Framework. *Cryst. Growth Des.* **2019**, *19* (12), 7096−7105.
(61) Kim, Y. J.; Jung, D. Y. Conformation Change of the Cyclohexanedicarboxylate Ligand toward 2D and 3D La(III)-Organic Coordination Networks. *Chem. Commun.* **2002**, *2* (8), 908−909.
(62) Cui, Z.; Zhang, X.; Liu, S.; Zhou, L.; Li, W.; Zhang, J. Anionic Lanthanide Metal-Organic Frameworks: Selective Separation of Cationic Dyes, Solvatochromic Behavior, and Luminescent Sensing of Co(II) Ion. *Inorg. Chem.* **2018**, *57* (18), 11463−11473.
(63) Huang, J. J.; Yu, J. H.; Bai, F. Q.; Xu, J. Q. White-Light-Emitting Materials and Highly Sensitive Detection of Fe3+ and Polychlorinated Benzenes Based on Ln-Metal-Organic Frameworks. *Cryst. Growth Des.* **2018**, *18* (9), 5353−5364.
(64) Su, S.; Chen, W.; Qin, C.; Song, S.; Guo, Z.; Li, G.; Song, X.; Zhu, M.; Wang, S.; Hao, Z.; Zhang, H. Lanthanide Anionic Metal-Organic Frameworks Containing Semirigid Tetracarboxylate Ligands: Structure, Photoluminescence, and Magnetism. *Cryst. Growth Des.* **2012**, *12* (4), 1808−1815.
(65) Li, Y. J.; Wang, Y. L.; Liu, Q. Y. The Highly Connected MOFs Constructed from Nonanuclear and Trinuclear Lanthanide-Carboxylate Clusters: Selective Gas Adsorption and Luminescent pH Sensing. *Inorg. Chem.* **2017**, *56* (4), 2159−2164.
(66) Wu, Y. P.; Xu, G. W.; Dong, W. W.; Zhao, J.; Li, D. S.; Zhang, J.; Bu, X. Anionic Lanthanide MOFs as a Platform for Iron-Selective Sensing, Systematic Color Tuning, and Efficient Nanoparticle Catalysis. *Inorg. Chem.* **2017**, *56* (3), 1402−1411.
(67) Pan, Y.; Su, H. Q.; Zhou, E. L.; Yin, H. Z.; Shao, K. Z.; Su, Z. M. A Stable Mixed Lanthanide Metal-Organic Framework for Highly Sensitive Thermometry. *Dalton Transactions* **2019**, *48* (11), 3723−3729.
(68) Yi, P.; Huang, H.; Peng, Y.; Liu, D.; Zhong, C. A Series of Europium-Based Metal Organic Frameworks with Tuned Intrinsic Luminescence Properties and Detection Capacities. *RSC Adv.* **2016**, *6* (113), 111934−111941.
(69) Ivanova, A. A.; Gontcharenko, V. E.; Lunev, A. M.; Sidoruk, A. V.; Arkhipov, I. A.; Taydakov, I. V.; Belousov, Y. A. New Carboxylate Anionic Sm-MOF: Synthesis, Structure and Effect of the Isomorphic Substitution of Sm3+ with Gd3+ and Tb3+ Ions on the Luminescent Properties. *Inorganics* **2022**, *10* (8), 104.
(70) Belousov, Yu. A.; Goncharenko, V. E.; Lunev, A. M.; Sidoruk, A. V.; Bezzubov, S. I.; Taidakov, I. V. New Heteroligand Europium and Gadolinium Formate Triazole Dicarboxylates: Synthesis, Structures, and Luminescence Properties. *Russ J. Coord Chem.* **2020**, *46* (6), 394−401.
(71) Atzori, C.; Ethiraj, J.; Colombo, V.; Bonino, F.; Bordiga, S. Adsorption Properties of Ce5 (BDC)7.5 (DMF)4 MOF. *Inorganics* **2020**, *8* (2), 9.
(72) Ouattara, L.; Diaco, T.; Bokra, Y. Influence of Water on the Anodic Oxidation Mechanism of Diethylenetriamine (Deta) on Platinum Electrode. *Bull. Chem. Soc. Eth.* **2006**, *20* (2), 269−277.
(73) Herlem, G.; Goux, C.; Fahys, B.; Dominati, F.; Gonçalves, A.-M.; Mathieu, C.; Sutter, E.; Trokourey, A.; Penneau, J.-F. Surface Modification of Platinum and Gold Electrodes by Anodic Oxidation of Pure Ethylenediamine. *J. Electroanal. Chem.* **1997**, *435* (1), 259−265.
(74) Long, Y.; Song, S.; Li, J.; Wu, L.; Wang, Q.; Liu, Y.; Jin, R.; Zhang, H. Pt/CeO $_2$ @MOF Core@Shell Nanoreactor for Selective Hydrogenation of Furfural via the Channel Screening Effect. *ACS Catal.* **2018**, *8* (9), 8506−8512.
(75) Chen, Y.; Huang, N.; Liang, Y. Preparation of CeO2/Cu-MOF/GO Composite for Efficient Electrocatalytic Oxygen Evolution Reaction. *Ionics* **2021**, *27*, 4347−4360.
(76) Casanova, D.; Llunell, M.; Alemany, P.; Alvarez, S. The Rich Stereochemistry of Eight-Vertex Polyhedra: A Continuous Shape Measures Study. *Chem. - Eur. J.* **2005**, *11* (5), 1479−1494.
(77) Blatov, V. A.; Shevchenko, A. P.; Proserpio, D. M. Applied Topological Analysis of Crystal Structures with the Program Package ToposPro. *Cryst. Growth Des.* **2014**, *14* (7), 3576−3586.
(78) Tsymbarenko, D.; Grebenyuk, D.; Burlakova, M.; Zobel, M. Quick and Robust PDF Data Acquisition Using a Laboratory Single-Crystal X-Ray Diffractometer for Study of Polynuclear Lanthanide Complexes in Solid Form and in Solution. *J. Appl. Crystallogr.* **2022**, *55* (4), 890−900.
(79) Wu, Z.; Li, M.; Overbury, S. H. On the Structure Dependence of CO Oxidation over CeO2 Nanocrystals with Well-Defined Surface Planes. *J. Catal.* **2012**, *285* (1), 61−73.
(80) Ha, H.; Yoon, S.; An, K.; Kim, H. Y. Catalytic CO Oxidation over Au Nanoparticles Supported on CeO2 Nanocrystals: Effect of the Au-CeO2 Interface. *ACS Catal.* **2018**, *8* (12), 11491−11501.
(81) He, X.; Looker, B. G.; Dinh, K. T.; Stubbs, A. W.; Chen, T.; Meyer, R. J.; Serna, P.; Román-Leshkov, Y.; Lancaster, K. M.; Dincă, M. Cerium(IV) Enhances the Catalytic Oxidation Activity of Single-Site Cu Active Sites in MOFs. *ACS Catal.* **2020**, *10* (14), 7820−7825.
(82) Lin, A.; Ibrahim, A. A.; Arab, P.; El-Kaderi, H. M.; El-Shall, M. S. Palladium Nanoparticles Supported on Ce-Metal Organic Framework for Efficient CO Oxidation and Low Temperature CO2 Capture. *ACS Appl. Mater. Interfaces* **2017**, *9* (21), 17961−17968.

https://doi.org/10.1021/acsomega.3c07906
ACS Omega 2023, 8, 48394−48404